Study of Phase Method in Tantalum Superconducting Qubit T_2^* Measurements

Hiu Yung Wong
Electrical Engineering
San Jose State University
San Jose, USA
hiuyung.wong@sjsu.edu

Kristin M. Beck
Quantum Coherent Device Physics Group
Lawrence Livermore National Laboratory
Livermore, CA
beck37@llnl.gov

Vito Mariano Iaia
Quantum Coherent Device Physics Group
Lawrence Livermore National Laboratory
Livermore, CA
iaia1@llnl.gov

Anika Zaman
Electrical Engineering
San Jose State University
San Jose, USA
anika.zaman@sjsu.edu

Yaniv Jacob Rosen
Quantum Coherent Device Physics Group
Lawrence Livermore National Laboratory
Livermore, CA
rosen10@llnl.gov

2024 IEEE International Conference on Quantum Computing and Engineering (QCE) | 979-8-3315-4137-8/24/$31.00 ©2024 IEEE | DOI: 10.1109/QCE60285.2024.00154

***Abstract*—In this paper, the phase method is proposed to measure the T_2^* dephasing time in a Tantalum-based superconducting qubit. In the regular Ramsey method for T_2^* measurement, a superposition state precesses on the equatorial plane of the Bloch-sphere due to detuning. The dephasing during the precession is recorded. In the phase method, rapid rotation is applied to rotate the superposition state on the equatorial plane through various angles (phases) to extract the dephasing during an idle time right before the rotation. While the phase method has been used in atomic physics, it has not been commonly used to characterize T_2^* in superconducting qubits. Compared to the traditional Ramsey method, the phase method does not require prior knowledge of the dephasing envelope, enabling it to capture the dynamic dephasing behavior of a qubit during the measurement more easily. It also does not rely on detuning and, thus, is insensitive to any detuning error. In this paper, a Tantalum-based superconducting qubit with a high T_1 ($\sim 220\mu s$) is used. After careful calibrations, extensive dephasing experiments were conducted using both the Ramsey and the phase methods to extract T_2^*. We show that the phase method is insensitive to detuning and works well even with a very sparse phase sampling (with a step size as large as $\frac{\pi}{2}$). We also show that, statistically, it is equivalent to the Ramsey method within $\pm 10\%$. Therefore, if both the Ramsey method and the phase method are used together, it is expected a more accurate and reliable T_2^* extraction is possible.**

***Index Terms*—Decoherence, Dephasing, T_2^*, T_ϕ, Quantum Computing, Superconducting Qubit**

I. Introduction

Using the gate model, quantum computers are promising to solve some critical engineering problems exponentially faster than classical approaches such as in prime factorization [1] and solving systems of linear equations [2] [3]. However, gate model quantum computing is only expected to be successful with error-free quantum bits (qubits). This is because gate model-based quantum computing algorithms rely on interference which has a very stringent requirement on qubit error rate [4] [5]. While error-free logical qubits may be achieved through error correction codes and circuitry [6] [7] and the overall errors can be further mitigated by machine learning techniques [8] [9], it is desirable to enhance the coherence time of a physical qubit to reduce the resources and computation times required for error correction. This is particularly important in the current Noisy Intermediate-Scale Quantum (NISQ) era [10], where error correction is generally not available.

Two of the most important coherence times of a qubit is the T_1 and T_ϕ times. T_1 is also called the energy relaxation time or the longitudinal relaxation time and T_ϕ is the dephasing time or transverse relaxation time [11] [12]. T_ϕ is usually much smaller than T_1 and limits the number of quantum gates that can operate before the information of the state is lost. T_1 measurement is straightforward by exciting a qubit in the ground state to an excited state and observing its decay rate. T_ϕ cannot be directly measured because the effect from energy relaxation cannot be decoupled. In an experiment, another quantity, T_2^*, is measured and is related to T_1 and T_ϕ through the following equation [13]:

$$\frac{1}{T_2^*} = \frac{1}{2T_1} + \frac{1}{T_\phi} \tag{1}$$

The Ramsey method has been commonly used for superconducting qubit T_2^* measurement. It relies on frequency detuning during the formation of a superposition state to have it rotate on the equatorial plane of the Bloch sphere. The dephasing during the rotation is recorded and displayed as a decaying profile in the experimental data which, however, also contains a sinusoidal envelope of the detuning frequency in its simplest form. In reality, it is often to see different envelopes such as beating due to system parity state switching or differently colored noise. Therefore, it is sensitive to the detuning frequency and also requires an accurate prior knowledge of the envelope function (i.e. is the envelope a simple sinusoidal function?) to obtain accurate and meaningful fitting and T_2^* extraction.

The phase method, which has been commonly used in atomic physics [14] [15] [16], on the other hand, is insensitive

979-8-3315-4137-8/24/$31.00 ©2024 IEEE
DOI 10.1109/QCE60285.2024.00154

to detuning and does not require prior knowledge of the envelope. The superposition state is first idle for a given time. Dephasing as a function of idle time is extracted and displayed as a decaying profile in the experimental data. This is made possible by applying a fast and well-controlled equatorial rotation at various angles (phases) immediately after the idle time. Through phase contrast measurement (finding the peak-to-peak measurement probability amplitude after a full 2π rotation), the amount of dephasing during the idle time can be found.

In the following sections, we will first discuss the calibration process of the system followed by a review of the Ramsey method. Then the phase method is introduced. Finally, its sensitivity to detuning and phase step size will be discussed and its equivalency to the Ramsey method will be demonstrated.

II. Experiment

Figure 1 shows a schematic of the system used in the experiment. A tantalum transmon is used in this study [17] [18]. The device is cooled to 10mK in a Bluefors dilution refrigerator (LD-400). The device is connected to an on-chip resonator in a package. The package is then connected to a Quantum Machine OPX [19] by co-axial cables through various temperature stages. Input signals are generated by a heterodyne readout circuit and output signals are collected using Quantum Machine OPX modulated and demodulated by a Holzworth local oscillator. Table I shows the parameters used in the experiment.

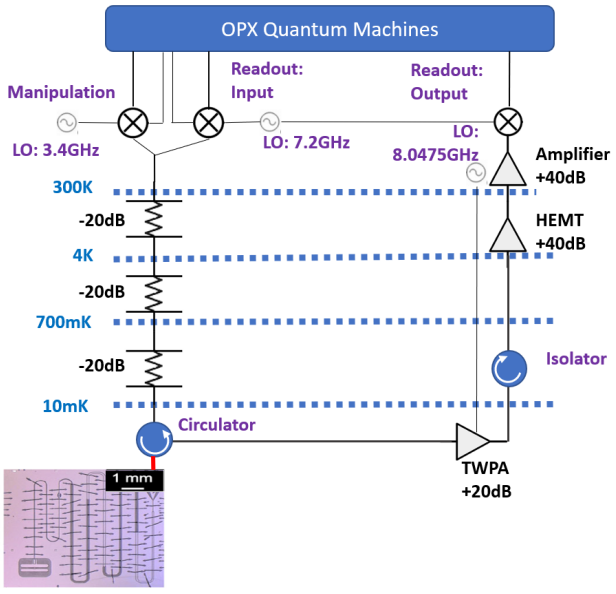

Fig. 1. Schematic of the system. The micrograph (modified from [17]) of the transmon qubit and resonator is shown.

The T_1 energy relaxation time and T_ϕ dephasing time are extracted from the experiment through the measurement of T_1 and T_2^* using Eq. (1).

TABLE I
Qubit readout and manipulation parameters used in this study.

Parameters	$\|0\rangle/\|1\rangle$	$\|1\rangle/\|2\rangle$	Readout	TWPA
LO (GHz)	3.4	3.4	7.2	8.0475
IF (MHz)	48.15434	-160.172099	46.13345	N/A
π-pulse Length (ns)	72	72	N/A	N/A
π-pulse Amplitude (mV)	183.3	69.5	N/A	N/A
Readout Pulse Length (ns)	N/A	N/A	252	N/A
Readout Pulse Amplitude (mV)	N/A	N/A	70	N/A
LO Power (dB)	N/A	N/A	N/A	-2.85

A. Readout Calibration and Correction

The accuracy of the extraction of T_1 and T_2^* depends on the state preparation fidelity and readout fidelity. The preparation and readout fidelity cannot be decoupled [20]. To increase the accuracy, calibration of the $I-Q$ plane is performed. $|0\rangle$ is prepared through thermal reset by waiting for $1ms$ which is about $5T_1$. $|1\rangle$ is obtained by applying a π-pulse (i.e. $72ns$, see Table I) to the thermally reset $|0\rangle$. They are measured and plotted on the $I-Q$ plane with $100,000$ identical experiments performed. The data is then classified using the Gaussian Mixture Model (GMM) [22] to find an optimal readout strategy and construct a confusion matrix to correct readout errors in the following experiments. A readout fidelity near 99% can be obtained as has been shown in past work [21]. Fig. 2 shows the $I-Q$ plane and the fitted negative log-likelihood predicted by GMM. The confusion matrix for $|0\rangle$ / $|1\rangle$ measurement is

$$M_{C,01} = \begin{pmatrix} 0.949 & 0.051 \\ 0.061 & 0.939 \end{pmatrix}. \tag{2}$$

Since thermal reset takes a long time, active reset is preferred. In active reset, a π-pulse is applied to obtain $|0\rangle$ when a state is measured to be $|1\rangle$ instead of waiting for it to decay thermally. This is possible with the aforementioned calibration.

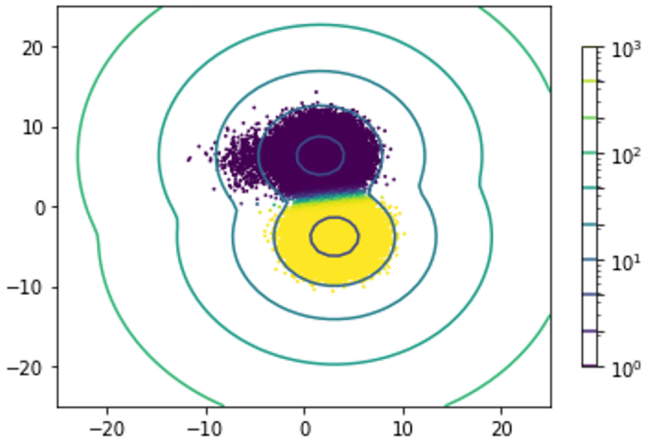

Fig. 2. The negative log-likelihood predicted by GMM for $|0\rangle$ / $|1\rangle$ readout.

The system being used is capable of qutrit operations [18]. This means that the qubit can be excited to $|2\rangle$ state under a well-controlled environment in addition to $|0\rangle$ and $|1\rangle$. Table I shows the corresponding parameters for $|1\rangle / |2\rangle$ transition. As will also be shown later, in some experiments, the qubit can be erroneously promoted to $|2\rangle$. Therefore, it is desirable to study and calibrate its qtrit read-out strategy. The same strategy as in the aforementioned $|0\rangle / |1\rangle$ calibration is used to obtain the distribution of $|0\rangle$ and $|1\rangle$ readout result on the $I-Q$ plane. To calibrate the readout of $|2\rangle$, the qubit is thermally reset after waiting for $4ms$ and is then excited to $|2\rangle$ by applying a π-pulse for $|0\rangle / |1\rangle$ transition (i.e. $72ns$) followed by a π-pulse for $|1\rangle / |2\rangle$ transition (also $72ns$ but at a different frequency, see Table I) and measured. 100,000 experiments are conducted. Fig. 3 shows the $I-Q$ planes and the fitted negative log-likelihood predicted by GMM for each state. The confusion matrix for $|0\rangle / |1\rangle / |2\rangle$ measurement is

$$M_{C,012} = \begin{pmatrix} 0.959 & 0.037 & 0.003 \\ 0.055 & 0.903 & 0.042 \\ 0.041 & 0.068 & 0.891 \end{pmatrix} \tag{3}$$

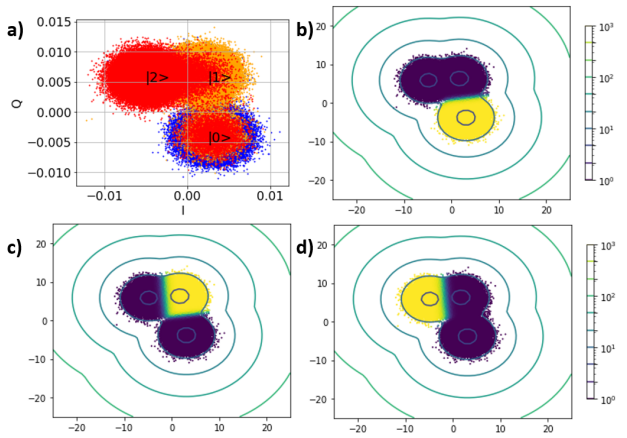

Fig. 3. a) Distribution of $|0\rangle$, $|1\rangle$, and $|2\rangle$ among the 100,000 readout data on the $I-Q$-plane in calibration. b), c), and d) show the negative log-likelihood predicted by GMM for $|0\rangle$, $|1\rangle$, and $|2\rangle$ states, respectively.

B. T_1 Measurement

T_1 is obtained by measuring the decay time from the excited state to the ground state. For example, to measure the T_1 of $|0\rangle / |1\rangle$ transition, the qubit is brought to the ground state $|0\rangle$ through active reset and then is excited to $|1\rangle$ by applying a π-pulse (i.e. $72ns$, see Table I). The qubit is then measured at different delay times, t, from $16ns$ to $1.6ms$ at a step of $40\mu s$. 1000 identical experiments (shots) are performed at each delay. The probability of measuring $|1\rangle$, $P_1(t)$, is then plotted against the delay and fitted using,

$$P_1(t) = P_1(0)e^{-\frac{t}{T_1}} \tag{4}$$

$P_1(0)$ is set to be 1. Fig. 4 shows an example of T_1 measurement and its fitting. The extracted T_1 is $222\mu s$.

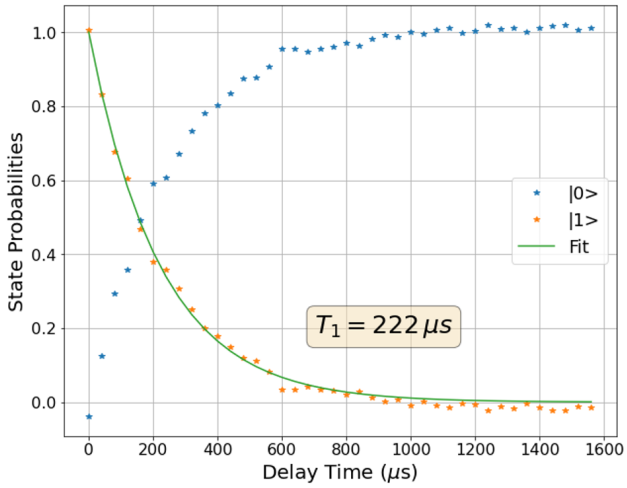

Fig. 4. An example of $|0\rangle / |1\rangle$ T_1 measurement. The probabilities have been corrected using the confusion matrix for more accurate extraction, resulting in small negative values at a large delay time.

C. T_2^* Measurements

Two methods are used to measure T_2^*. One is the regular Ramsey method (dubbed "the Ramsey method"). Another is a method commonly used in atomic physics and is dubbed "the phase method".

1) Ramsey Method for T_2^* Measurement: Ramsey method is commonly used to measure the T_2^* of a qubit. As shown in Fig. 5, firstly, the qubit is initialized through an active reset (Fig. 5a). Then a $\frac{\pi}{2}$-pulse for $|0\rangle / |1\rangle$ transition (i.e. $36ns$, see Table I) is applied with a detuning frequency, δ_f, of 0.6MHz. This will bring the qubit to a superposition state of $\frac{|0\rangle+|1\rangle}{\sqrt{2}}$ (Fig. 5b). Due to detuning, the qubit will precess on the Bloch sphere (Fig. 5c, e). After precessing for time t, another $\frac{\pi}{2}$-pulse is applied. Depending on the position of the state on the equator, the $\frac{\pi}{2}$-pulse will bring the state to $|0\rangle$ (e.g. Fig. 5f), $|1\rangle$, or a superposition state of $|0\rangle$ and $|1\rangle$ (e.g. Fig. 5d). If a measurement follows, the probability of measuring $|0\rangle$, $P_1(t)$, oscillates as a function of t. When there is phase decoherence, the Bloch vector shrinks (Fig. 5g, h), and the amplitude of the oscillation decreases as a function of t. t is varied from $16ns$ to $80\mu s$ in steps of $200ns$. To measure the probabilities, for each precess time, t, the experiment is repeated 1000 times. For a dephasing process with a single time constant, the decay of the amplitude can be modeled as

$$P_1(t) = a + be^{-\frac{t}{T_2^*}} \cos\left(2\pi\delta_f t + \phi\right) \tag{5}$$

where ϕ, a and b are fitting parameters and a and b are expected to be $\frac{1}{2}$ in theory.

Fig. 6 shows an example of the Ramsey measurement obtained from this system. The fitting parameters are $a = 0.47$, $b = 0.55$, $T_2^* = 27.2$, $\delta_f = 0.40MHz$, and $\phi = 0.051rad$. The curve can be fitted well with one single time constant in the experimental interval ($80\mu s$) and the extracted T_2^* is $39\mu s$.

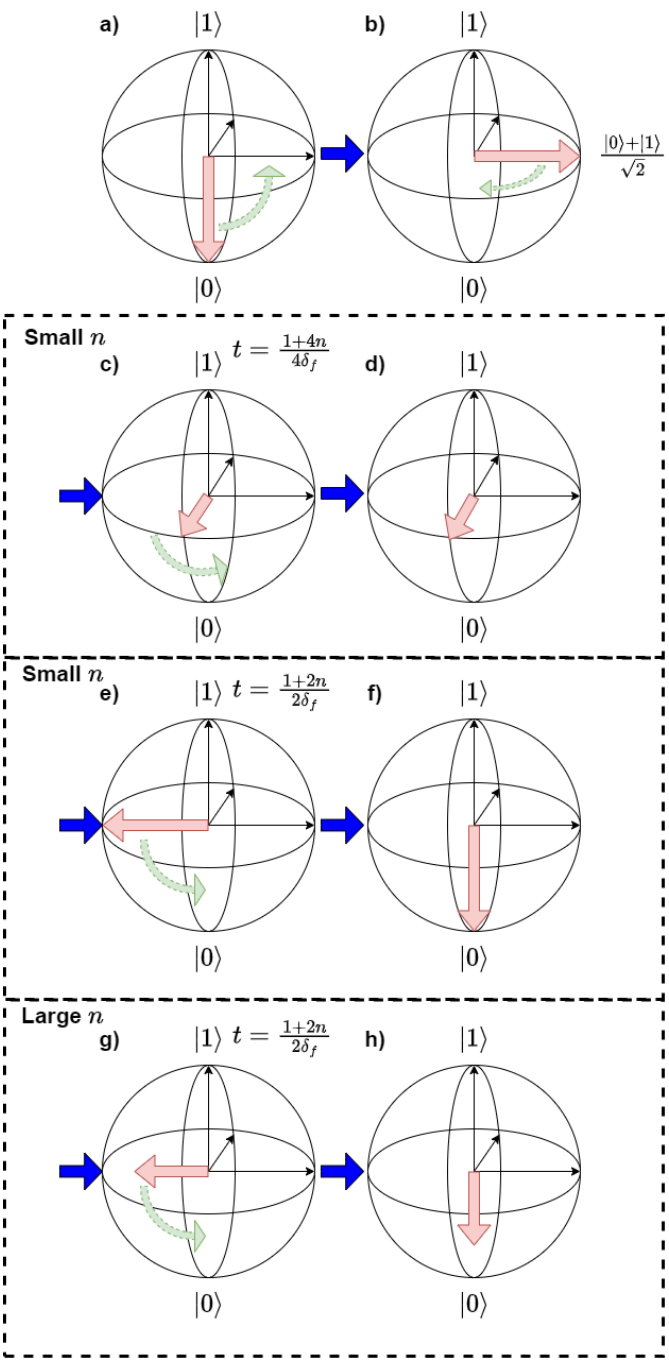

Fig. 5. Bloch spheres depicting the Ramsey measurement process. Pink arrows represent the Bloch vectors. Green arrows represent the subsequent operations on the Bloch vector. n is the number of completed circles of precessing and the precessing angle varies from 0 to 2π with $\frac{\pi}{2}$ and π as examples. From b), due to detuning, the vector will precess to c), e), or g). When n is small, dephasing is not much. g) is the case when n is large and the Bloch vector has shrunk noticeably.

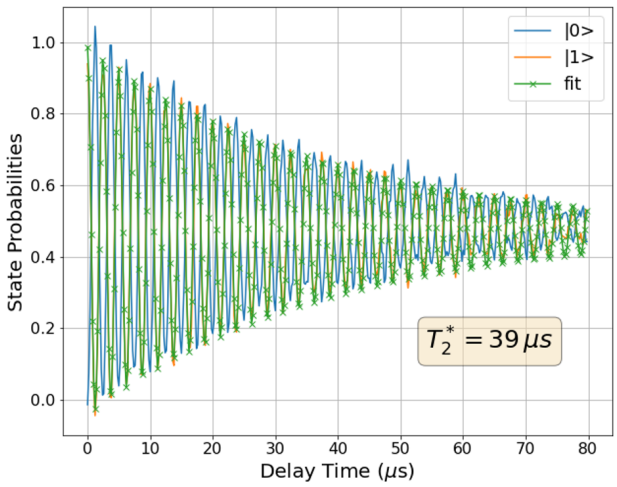

Fig. 6. Ramsey $|0\rangle$ / $|1\rangle$ T_2^* measurement result example with a long T_2^* which can be fitted well using a single time constant.

However, when multiple experiments are performed on different days, T_2^* may change due to the drifting of the environment including the changing of charge parity [18] [23]. T_2^* might not be fitted well with one time constant. For example, Fig. 7 shows that while the fitting error of the full curve is minimized, it cannot fit the peak-to-peak range between $0\mu s$ and $40\mu s$ well.

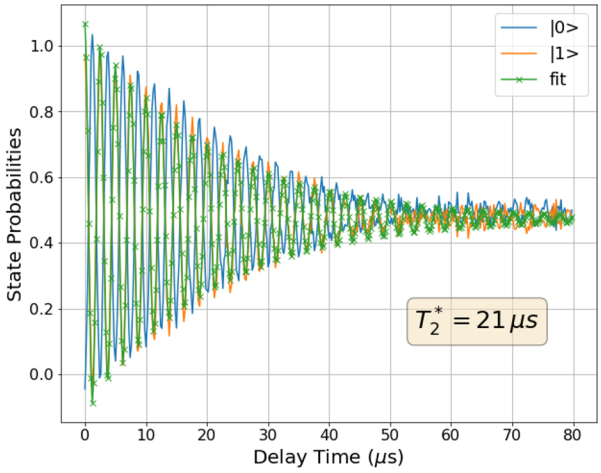

Fig. 7. Ramsey $|0\rangle$ / $|1\rangle$ T_2^* measurement result example with a short T_2^* which cannot be fitted well using a single time constant, particularly in the $0\mu s$ to $40\mu s$ region.

On the other hand, if only the first $24\mu s$ of the curve is fitted (Fig. 8), the first $24\mu s$ of the curve is fitted well and the extracted T_2^* is $28\mu s$. This example shows that if there are more than one time constant in the Ramsey experiment, it is difficult to extract a meaningful T_2^* as accurate prior knowledge of the envelope is not available. Significant data processing (such as filtering) and analysis are required before the fitting.

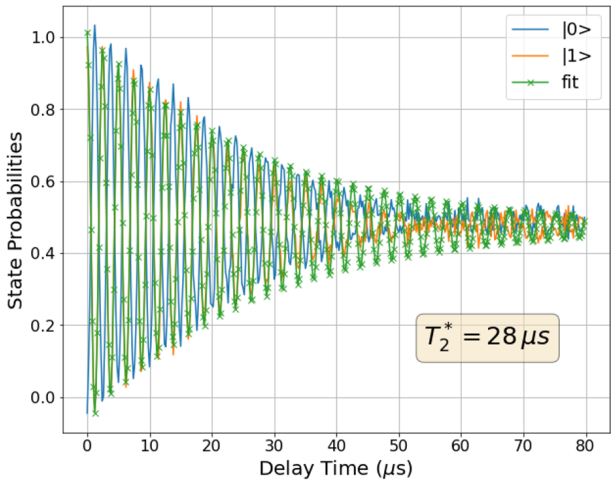

Fig. 8. Ramsey $|0\rangle$ / $|1\rangle$ T_2^* measurement result example with a short T_2^*. This is the same figure as Fig. 7 except that only the first $24\mu s$ (orange line) data is used in the fitting.

2) Phase Method for T_2^* Measurement: Like the Ramsey method, the qubit is initialized to $|0\rangle$ through active reset (Fig. 9a) and brought to a superposition state of $\frac{|0\rangle+|1\rangle}{\sqrt{2}}$ (Fig. 9b) with a $\frac{\pi}{2}$-pulse for $|0\rangle$ / $|1\rangle$ transition (i.e. $36ns$, see Table I). Unlike the Ramsey method, detuning is not required to extract the T_2^* of $|0\rangle$/$|1\rangle$. Therefore, this methodology is expected to be insensitive to detuning errors. Without detuning, the vector will not precess on the equatorial plane. The system is then idle for a time, t, from $16ns$ to $80\mu s$ in steps of $200ns$ before a rotation about the vertical axis is applied (Fig. 9c). The rotation is accomplished by a virtual Z-gate operation through coordinate transformation without an actual gate pulse. The Bloch vector is rotated for an angle (phase, p) from 0 to $\frac{11\pi}{6}$ in steps of $\frac{\pi}{6}$. As in the Ramsey method, another $\frac{\pi}{2}$-pulse is applied after the virtual Z-gate (Fig. 9d). Depending on the position of the state on the equatorial plane, the $\frac{\pi}{2}$-pulse will bring the state to $|0\rangle$ (Fig. 9e), $|1\rangle$, or a superposition state of $|0\rangle$ and $|1\rangle$. If a measurement follows, the probability of measuring $|1\rangle$ at a given t, $P_1(p)$, oscillates as a function of p and is sinusoidal with a peak-to-peak amplitude, A. When there is dephasing and t is large, the Bloch vector will have shrunk during the idle time (Fig. 9f, g, h). Note that since the virtual Z-gate operation and the $\frac{\pi}{2}$-pulse are short compared to t (except for $t = 16ns$ and $t = 416ns$), we can assume that dephasing occurs only during the idle time and the Bloch vector only shrinks (Fig. 5f) during that time to simplify the calculations. The peak-to-peak amplitude of the sinusoidal oscillation, A, decreases as a function of t due to the shrinkage. To measure the probabilities, for each delay time, t, and each phase, p, the experiment is repeated 1000 times.

Fig. 10 shows three examples of $P_1(p)$ vs. p taken at $t = 0\mu s$, $12\mu s$, and $24\mu s$. The amplitude, A, is extracted by fitting to

$$P_1(p) = \frac{A}{2}\cos(p+\phi) + o \qquad (6)$$

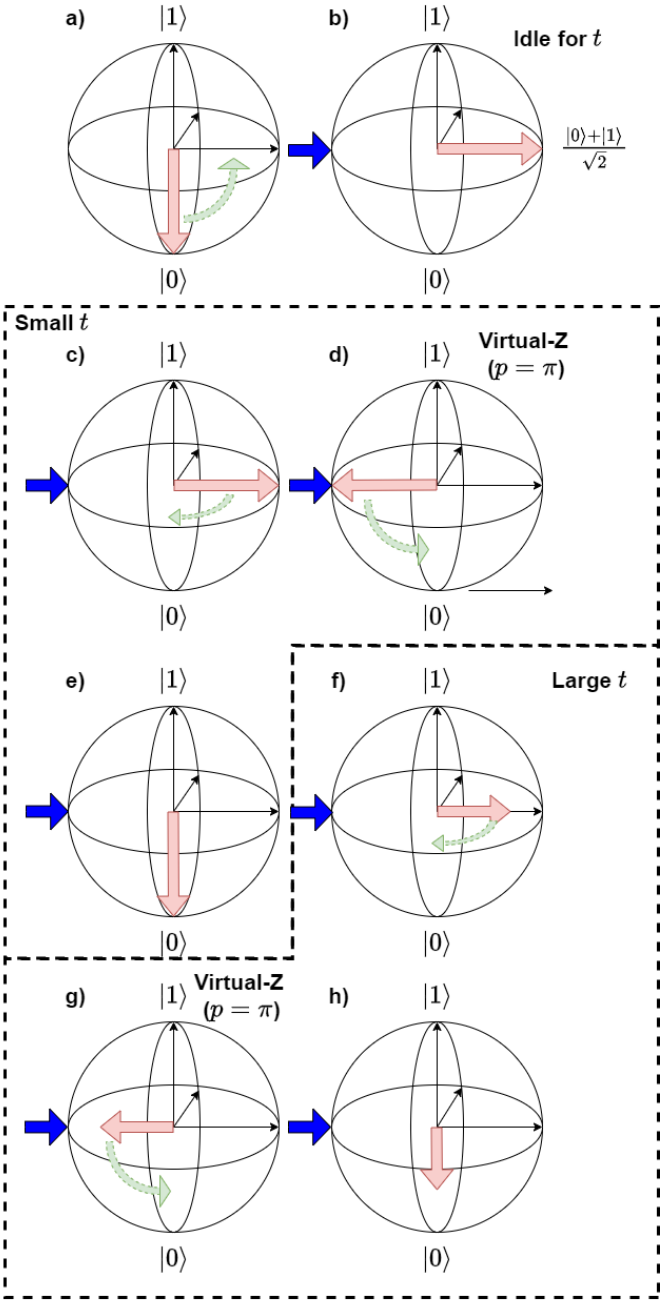

Fig. 9. Bloch spheres depicting the T_2^* measurement using the phase method. Pink arrows represent the Bloch vectors. Green arrows represent the subsequent operations on the Bloch vector. The state is initialized in a) followed by a $\frac{\pi}{2}$-pulse to b). After being idle for time t, a virtual Z-gate is applied. If t is small, the Bloch vector will not have a noticeable shrink (c-e). If t is large, the vector would have shrunk before the application of the virtual Z-gate (f-h). Measurements are performed after e) and h). p varies from 0 to 2π. $p = \pi$ is used as an example.

where ϕ and o are other fitting parameters. In theory, $o = 0.5$ and ϕ is the initial phase of the sinusoidal curve.

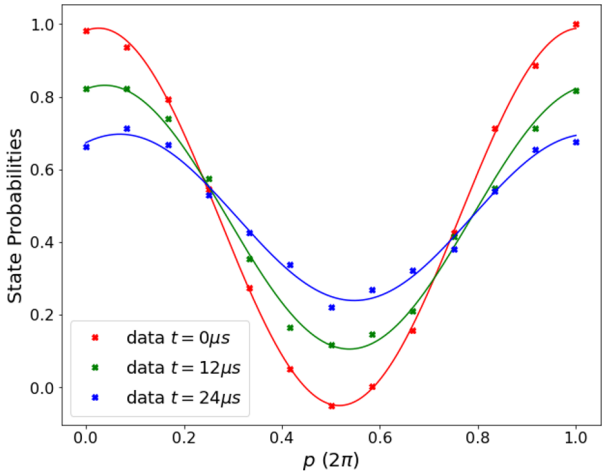

Fig. 10. P_1 as a function of p at various idle time, t, (markers) and their fitting curves (lines).

A is then plotted against t and modeled as,

$$A(t) = A(0)e^{-\frac{t}{T_2^*}} \tag{7}$$

In theory, $P_1(0)$ is expected to be 1. A phase method experiment is run immediately after the Ramsey experiment in Fig. 6 and it is shown in Fig. 11. The phase method clearly shows that even in this long T_2^* process, it has multiple time constants, although they are similar such that it is not discernible in the Ramsey method. Based on visual inspection, the first $40\mu s$ data which visually follows the same time constant is used for fitting. The extracted T_2^* is $37\mu s$ which is very similar to that extracted using the Ramsey method ($39\mu s$ in Fig. 6). This shows the validity of the phase method and also its ability to unveil hidden structures.

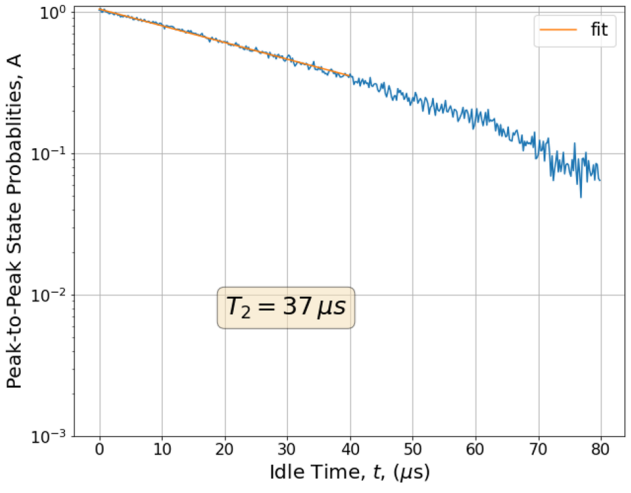

Fig. 11. T_2^* extraction using phase method run immediately after the experiment in Fig. 6. The first $40\mu s$ (orange line) data which visually follows the same time constant is used for fitting.

Immediately after the experiment in Fig. 7 and Fig. 8, a phase method experiment is also conducted. Figure 12 shows the results and its fitting. Only the first $24\mu s$ data is used for the fitting as they appear to follow the same time constant. This is the same as what is used in Fig. 8. The extracted T_2^* is $28\mu s$ and is the same as the Ramsey method in Fig. 8.

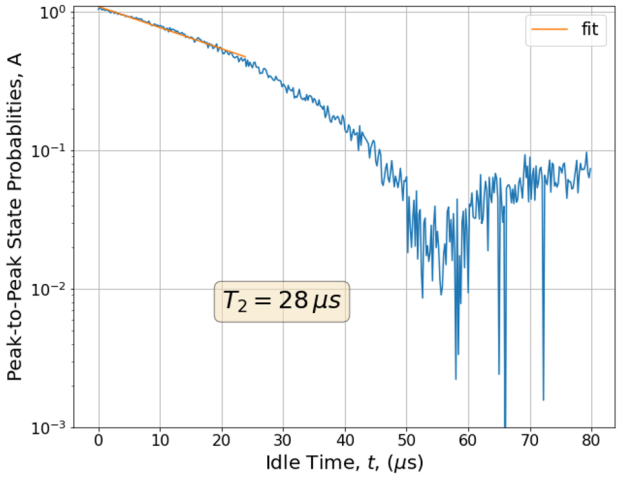

Fig. 12. T_2^* extraction using phase method run immediately after the experiment in Fig. 7 and Fig. 8. The first $24\mu s$ (orange line) data is used for fitting.

III. Further Experiments

A. Effect of Detuning

As mentioned earlier, the phase method does not require detuning and it relies on the applications of the virtual-Z gates to rotate the superposition states on the Bloch sphere equatorial plane. Since phase contrast is used to measure the peak-to-peak amplitude, A, in Eq. 6 and Eq. 7, it also does not matter if the superposition state precesses. A precessing superposition state will elongate the sinusoidal curves horizontally (as it adds additional rotation). However, as long as it does not precess too much during the time Z-gate operates, A can still be captured accurately. Since virtual-Z gate is used, it consumes essentially no time in the operation. As a result, precession due to detuning would not even distort the sinusoidal curve to be fitted by Eq. 6.

Fig. 13 plots $P_1(p)$ vs. p with a detuning of 1MHz for all t from $t = 0\mu s$ to $80\mu s$. Unlike Fig. 10 where $P_1(p)$ of different times have a similar initial phase (ϕ in Eq. 6), the initial phase drifts as a function of time. However, this does not prevent it from measuring T_2^* successfully.

Fig. 14 shows the plot of $A(t)$ and the extracted T_2^* to be $44\mu s$. Note that this set of experiments was taken on a different date than the aforementioned ones which explains the difference in T_2^* values.

B. Effect of Phase Sampling Rate

To further test the robustness of the phase method, different sampling rates were also experimented. In the previous experiments, p between 0 and 2π was sampled uniformly with a

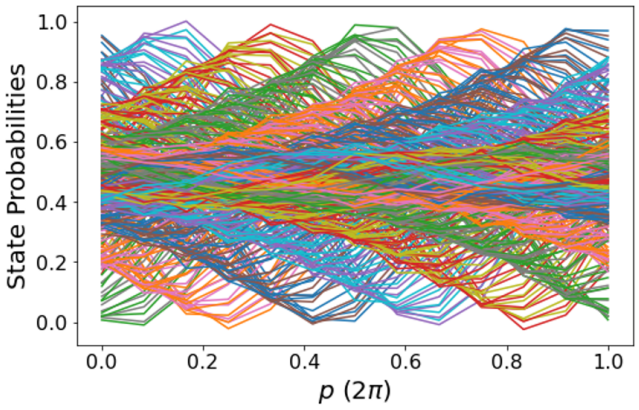

Fig. 13. P_1 as a function of phase p at various t with a detuning of $1MHz$. Curves taken at different time delays t are colored differently for clarity.

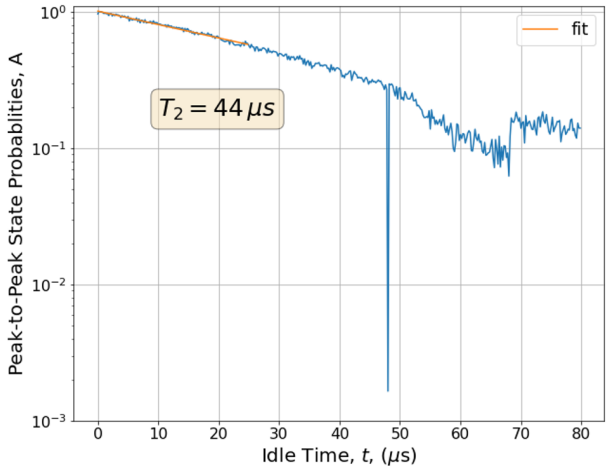

Fig. 14. T_2^* extraction using phase method using the data in Fig. 13.

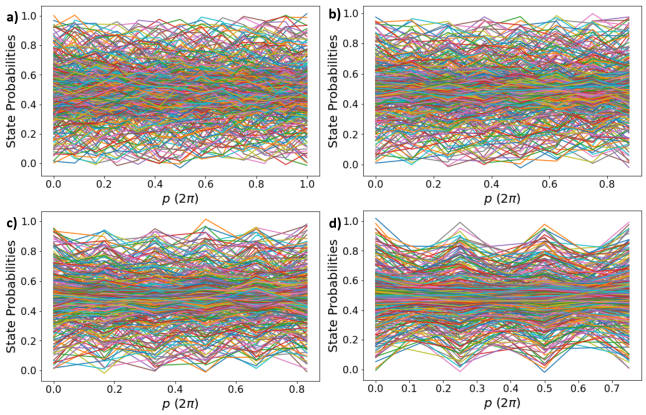

Fig. 15. P_1 as a function of phase p at various phase sampling rate. a), b), c), and d) has $m = 12$, 8, 6, and 4, respectively.

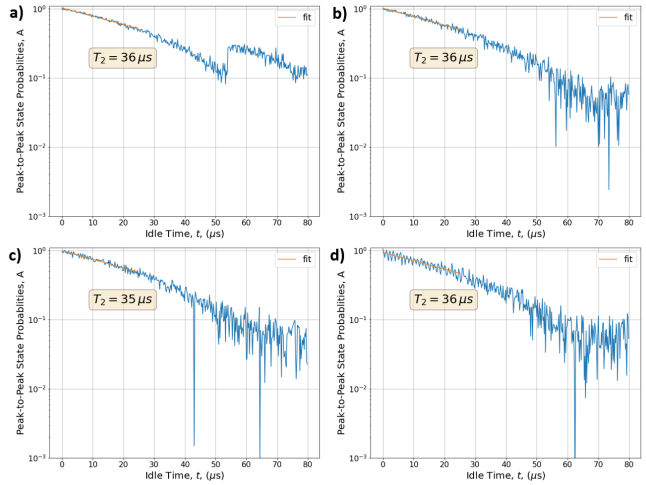

Fig. 16. T_2^* extraction using phase method using the data in Fig. 15. a), b), c), and d) have $m = 12$, 8, 6, and 4, respectively.

spacing of $\frac{2\pi}{12}$. Here, a spacing of $\frac{2\pi}{m}$ with $m = 12$, 8, 6, and 4 are investigated.

Fig. 15 plots $P_1(p)$ vs. p (no detuning) all t from $t = 0\mu s$ to $80\mu s$ for $m = 12$, 8, 6, and 4. It can be seen that when $m = 4$, the curves do not resemble sinusoidal curves at all. Fortunately, fitting using Eq. 6 is used to extract A. As a result, it is still able to capture the essential information of the data to perform meaningful phase contrast.

Fig. 16 shows the corresponding plots of $A(t)$ and the extracted $T_2^{*\prime}s$. The extracted T_2^* is essentially unchanged.

C. Statistical Comparison between the Ramsey and Phase Methods

To gain a statistical understanding of the relationship between the Ramsey and phase methods, more than 100 experiments were conducted over 84 hours. The phase method was conducted immediately after the Ramsey method to ensure that each T_2^* was measured under a similar environment. It should also be noted that the system is shared among various researchers. There is a possibility that the jobs from other experiments may be executed between the Ramsey and the phase method experiments in each pair. However, since jobs that will run more than 2 minutes are not encouraged to be submitted to the system, the delay time, if any, between the Ramsey and phase method experiments are expected to be short.

Due to glitches in the amplifier chain (Fig. 1), the readout occasionally may have errors. In this case, the data is discarded. Moreover, it is found in some experiments, some $|1\rangle$ states are excited to $|2\rangle$ states. Since the readout strategy is to classify $|1\rangle$ and $|0\rangle$ based on a partitioning line on the $I-Q$-plane (Fig. 2), some $|2\rangle$ states with low I values will be misclassified as $|0\rangle$.

For example, Fig. 17 shows one instance of such an error. Due to unknown reasons, $|2\rangle$ is populated. As a result, the probability of measuring $|1\rangle$ at $t = 0s$ is much smaller than 1 as shown in Fig. 18. Since the initial value of P_1 is small, this usually leads to an overestimation of T_2^* due to the more gentle slope.

The corresponding Ramsey measurement (Fig. 19), which was conducted right before the phase method, also shows a

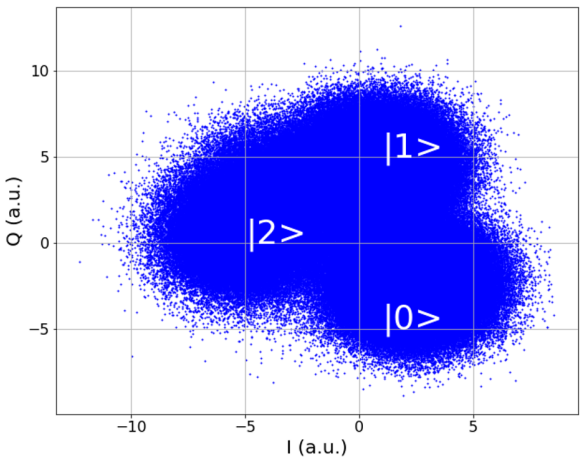

Fig. 17. $I - Q$ plot of the measurements of the first $8\mu s$ (orange line) in one of the phase method experiment. $|2\rangle$ is populated due errors.

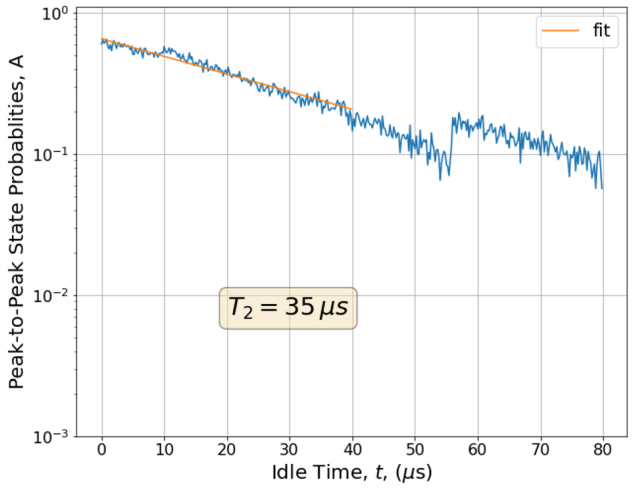

Fig. 18. Extraction of $|0\rangle$ / $|1\rangle$ T_2^* using phase method when $|2\rangle$ is populated inadvertently and when there is possible amplifier glitches. The $I - Q$ plot of the first $8\mu s$ (orange line) data is shown in Fig. 17.

similar issue in which P_1 is much smaller than the expected value of 1.

Besides removing the data with $P_1(0)$ much smaller than 1, there are also data that show "steps" in the phase method. An example is shown in Fig. 20 in which there is a sudden decrease of P_1 at $t = 20\mu s$. This is believed due to a glitch in the readout amplifiers. Data of this type are also discarded.

After removing the invalid data points, only 79 are left. Figure 21 shows the correlations between the Ramsey method and the phase method after the abnormal data are removed. It can be seen that 77 of the 79 T_2^* extracted using the phase method falls within $\pm 10\%$ of the T_2^* extracted using the Ramsey method.

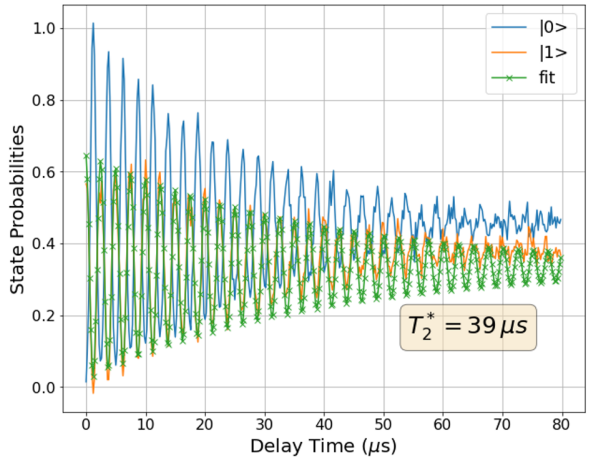

Fig. 19. Extraction of $|0\rangle$ / $|1\rangle$ T_2^* using Ramsey method when $|2\rangle$ is populated inadvertently and when there is possible amplifier glitches. This experiment was conducted right before that in Fig. 18.

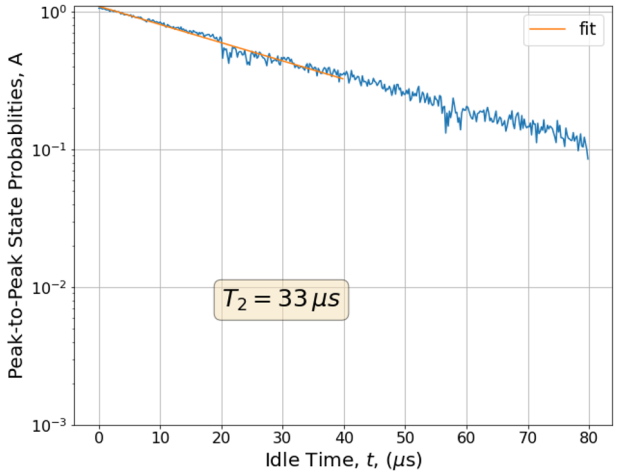

Fig. 20. Plotting of the T_2^* extracted using the phase method against the T_2^* extracted using the Ramsey method.

IV. Conclusions

The phase method is applied to a tantalum-based superconducting qubit to measure its T_2^*. It is found that the phase method gives a similar result to the Ramsey method. It does not rely on detuning and, thus, it is insensitive to detuning errors. By extracting the dephasing through phase contrast, the decay curve is clearer and easier to be comprehended and, unlike the Ramsey method, it does not require any prior knowledge of an envelope in the decay curve. It is also found that, due to its robustness, very sparse phase sampling is sufficient. Therefore, if both the Ramsey method and the phase method are used together, it is expected that a more accurate and reliable T_2^* extraction is possible.

Acknowledgment

This material is based upon work supported by the National Science Foundation under Grant No. 2125906. The authors

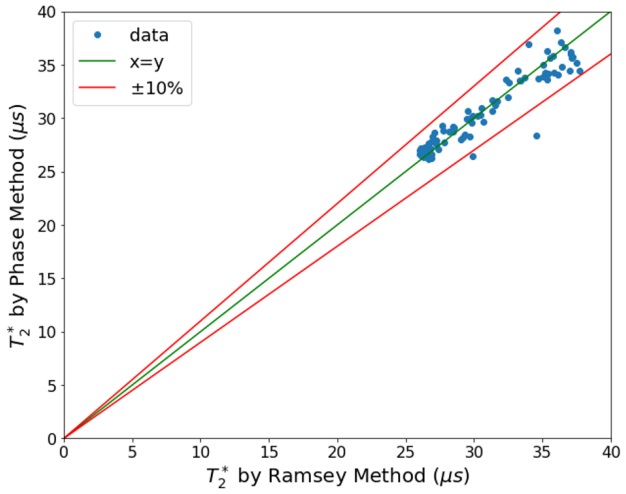

Fig. 21. Plotting of the T_2^* extracted using the phase method against the T_2^* extracted using the Ramsey method.

thank MITLL and IARPA for allowing us to use their TWPAs. Prepared in part by LLNL under Contract DE-AC52-07NA27344.

REFERENCES

[1] P. W. Shor, "Algorithms for quantum computation: Discrete logarithms and factoring," in Proc. 35th Annu. Symp. Found. Comput. Sci., Nov. 1994, pp. 124–134, doi: 10.1109/SFCS.1994.365700.

[2] A. W. Harrow, A. Hassidim, and S. Lloyd, "Quantum algorithm for linear systems of equations," Phys. Rev. Lett., vol. 103, no. 15, Oct. 2009, Art. no. 150502.

[3] Y. Cao, A. Daskin, S. Frankel, and S. Kais, "Quantum circuit design for solving linear systems of equations," Mol. Phys., vol. 110, nos. 15–16, pp. 1675–1680, Aug. 2012.

[4] A. Zaman, Hector Morrell, and Hiu Yung Wong, "A Step-by-Step HHL Algorithm Walkthrough to Enhance Understanding of Critical Quantum Computing Concepts," in IEEE Access, 2023. 10.1109/ACCESS.2023.3297658.

[5] A. Zaman and H. Y. Wong, "Study of Error Propagation and Generation in Harrow-Hassidim-Lloyd (HHL) Quantum Algorithm," 2022 IEEE Latin American Electron Devices Conference (LAEDC), 2022, pp. 1-4, doi: 10.1109/LAEDC54796.2022.9908231.

[6] P. W. Shor, "Scheme for reducing decoherence in quantum computer memory," Physical review A, vol. 52, no. 4, p. R2493, 1995.

[7] S. J. Devitt, W. J. Munro, and K. Nemoto, "Quantum error correction for beginners," Rep. Prog. Phys., vol. 76, no. 7, p. 076001, Jun. 2013, doi: 10.1088/0034-4885/76/7/076001.

[8] C. Kim, K. D. Park and J. -K. Rhee, "Quantum Error Mitigation With Artificial Neural Network," in IEEE Access, vol. 8, pp. 188853-188860, 2020, doi: 10.1109/ACCESS.2020.3031607.

[9] D. Cruz, F. A. Monteiro, and B. C. Coutinho, "Quantum Error Correction via Noise Guessing Decoding," *arXiv:2208.02744 [quant-ph]*, Aug. 4, 2022, revised Oct. 27, 2023, version 3.

[10] M. Kjaergaard, et al., "Superconducting qubits: Current state of play," Annual Review of Condensed Matter Physics 11 (2020): 369-395.

[11] Michael A. Nielsen and Isaac L. Chuang, Quantum Computation and Quantum Information: 10th Anniversary Edition. Cambridge University Press, 2011.

[12] Christopher J. Foot, Atomic Physics. Oxford University Press, 2005.

[13] M. Reagor, W. Pfaff, C. Axline, R. W. Heeres, N. Ofek, K. Sliwa, E. Holland, C. Wang, J. Blumoff, K. Chou, M. J. Hatridge, L. Frunzio, M. H. Devoret, L. Jiang, and R. J. Schoelkopf, Quantum memory with millisecond coherence in circuit qed, Phys. Rev. B 94, 014506 (2016).

[14] D. Adam, Q. Bouton, J. Nettersheim, S. Burgardt, and A. Widera, "Coherent and dephasing spectroscopy for single-impurity probing of an ultracold bath," Phys. Rev. Lett. 129, 120404 (2022).

[15] F. Schmidt, D. Mayer, Q. Bouton, D. Adam, T. Lausch, N. Spethmann, and A. Widera, "Quantum spin dynamics of individual neutral impurities coupled to a bose-einstein condensate," Phys. Rev. Lett. 121, 130403 (2018).

[16] C. Langer, R. Ozeri, J. D. Jost, J. Chiaverini, B. DeMarco, A. Ben-Kish, R. B. Blakestad, J. Britton, D. B. Hume, W. M. Itano, D. Leibfried, R. Reichle, T. Rosenband, T. Schaetz, P. O. Schmidt, and D. J. Wineland, "Long-lived qubit memory using atomic ions", Phys. Rev. Lett. 95, 060502 (2005).

[17] A. P. M. Place, et al., "New material platform for superconducting transmon qubits with coherence times exceeding 0.3 milliseconds," Nature Communications 12, 1779 (2021).

[18] D. M. Tennant, L. A. Martinez, K. M. Beck, S. R. O'Kelley, C. D. Wilen, R. McDermott, J. L. DuBois, and Y. J. Rosen, "Low-frequency correlated charge-noise measurements across multiple energy transitions in a tantalum transmon", PRX Quantum 3, 030307 (2022).

[19] Quantum Machines OPX. Accessed: Jan. 1, 2024. [Online]. Available: https://www.quantum-machines.co/products/opx/

[20] Benjamin Nachman, and Michael R. Geller, "Categorizing Readout Error Correlations on Near Term Quantum Computers", arXiv:2104.04607.

[21] Hiu Yung Wong, Prabjot Dhillon, Kristin Beck, and Yaniv Jacob Rosen, "A Simulation Methodology for Superconducting Qubit Readout Fidelity," Solid-State Electronics, Volume 201, March 2023, 108582. https://doi.org/10.1016/j.sse.2022.108582.

[22] GMM classification. Accessed: Jan. 1, 2024. [Online]. Available: https://scikit-learn.org/0.15/auto_examples/mixture/plot_gmm_classifier.html

[23] L. A. Martinez, Z. Peng, D. Appelö, D. M. Tennant, N. Anders Petersson, J. L DuBois, and Y. J. Rosen, "Noise-specific beating in the higher-level Ramsey curves of a transmon qubit," Appl. Phys. Lett. 122, 114002 (2023).